Oscillations in Shock-Induced Combustion near Conical Projectiles

Jimmy Verreault, Andrew J. Higgins
Department of Mechanical Engineering, McGill University, Montreal, H3A 2K6, Canada

1 Introduction

Combustion instabilities around hypersonic blunt projectiles traveling into a gaseous combustible mixture were observed experimentally in a number of studies in the 1960's and 1970's [1–3]. The observed flowfields were classified in two categories: the regular regime characterized by regular and high-frequency pulsations and the large-disturbance regime that referred to irregular and low-frequency pulsations. One-dimensional models were proposed by McVey and Toong [4] and Alpert and Toong [3] to describe the pulsation mechanism for the regular and large-disturbance regimes, respectively, based on wave interactions. Extensive numerical simulations were conducted in the 1990's to reproduce qualitatively the two regimes [5–7] and to reproduce the pulsation frequency for the regular regime [8–10]. Matsuo and Fujii [11] proposed a non-dimensional parameter (the first Damköhler number) to classify the combustion regimes and to predict them based on the experimental conditions.

Combustion instabilities produced by hypersonic conical projectiles were observed in the work of Toong [12] and Kasahara et al [13]. They assumed that the observed pulsations were equivalent to that produced by blunt bodies. In the present investigation, Schlieren photographs of combustion instabilities around hypersonic conical projectiles are presented. The prediction method using the first Damköhler parameter is used and compared with the results previously obtained by Matsuo and Fujii [11] with the blunt configuration.

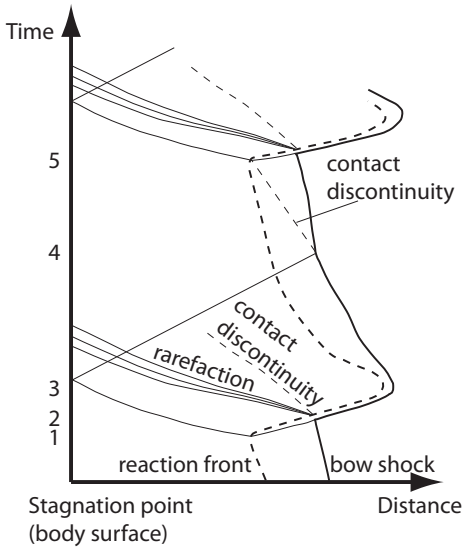

Figure 1: An $x-t$ diagram of the wave interaction model proposed by Matsuo and Fuji [6].

2 Theory

2.1 Wave interaction model

The one-dimensional wave interaction model for the large-disturbance regime, shown in Fig. 1, was originally proposed by Alpert and Toong [3] and later revised by Matsuo and Fujii [6]. The $x - t$ diagram describes the propagation

Correspondence to: jimmy.verreault@mail.mcgill.ca

of the different waves along the stagnation streamlines between the bow shock and the body surface. At time t_1, an explosion occurs at the reaction front, sending shock waves towards the body surface and the bow shock. The right-propagating shock interacts with the bow shock at t_2, forming a rarefaction wave and a contact discontinuity. The reaction front is closely coupled with the shock between t_1 and t_3. At t_3, the bow shock weakens and the reaction front decouples from it. The shock reflected from the body surface strengthens the bow shock at t_4, creating a contact discontinuity that separates a cold gas region (on the left of the discontinuity) and a hot gas region (on the right of the discontinuity). An explosion occurs at t_5 and a new cycle begins.

2.2 Prediction method of the combustion regime

To predict the type of flowfield induced by a blunt projectile without conducting experiments or numerical simulations, Matsuo and Fujii [11] proposed the use of the first Damköhler number defined as $Da = \tau_f/\tau_c$. The fluid time scale is given by $\tau_f = D/a_2$, where D is the projectile diameter and a_2 is the sound speed of the unburnt gas behind the bow shock. The fluid time scale thus corresponds to the time required for the waves to travel the distance of a projectile diameter. The chemical time scale is obtained from the integration of the zero-dimensional reactive flow equations. From this calculation, the maximum rate of temperature increase $(dT/dt)_{max}$ is used in the definition of the chemical time scale, $\tau_c = \frac{T_2}{(dT/dt)_{max}}$, where T_2 is the temperature of the unburnt gas behind the bow shock. The chemical time scale is thus a measure of the energy release intensity.

3 Experimental Apparatus

The projectiles were launched from a single stage, combustion-driven gas gun using hydrogen and oxygen as the propellant. This launcher is capable of velocities of 2700 m/s; the details of its design and operation are given by Verreault et al [14]. After passing through a section of launch tube with venting slots connected to an evacuated chamber to absorb the propellant gases from the launcher, the projectiles were injected through a very thin (13 m) Mylar diaphragm into a $2H_2$+O_2+7Ar mixture contained in the cylindrical test section (16.5 cm in diameter, 92 cm long) that was equipped with windows that permitted flow visualization. Schlieren photography using a high-speed framing camera (HSFC-Pro image-intensified camera) was employed to monitor the flowfield around the projectiles. The projectiles were 1.27 cm in diameter with cone half angles varying from 35° to 60°. To maintain the projectile velocity greater than 1 700 m/s with the launcher used, their maximum mass was limited to 4 g. A shallow cavity on the back of the projectile ensured sealing against the launch tube via internal pressurization, preventing blow-by of the propellant gas. The projectile carried an onboard NdFeB magnet used to trigger the camera and data acquisition system via a current induced in a coil positioned near the muzzle of the launcher. The projectile velocity was obtained by direct measurement from two photographs of the same experiment, taken at a known time interval apart. All projectile designs used in this investigation were aerodynamically unstable and would eventually tumble in flight (the gas gun had an unrifled, smooth bore launch tube). The test section windows were located 34 to 44 cm downstream of the muzzle; given this short distance of travel, canting of the projectile over this distance due to aerodynamic instability was negligible provided that the projectile exited the muzzle initially flying straight.

4 Results and Discussion

The Schlieren photographs showing the combustion instabilities from conical projectiles are presented in Fig. 2. The experimental conditions of the 6 firings are given in Table 1. Combustion instabilities

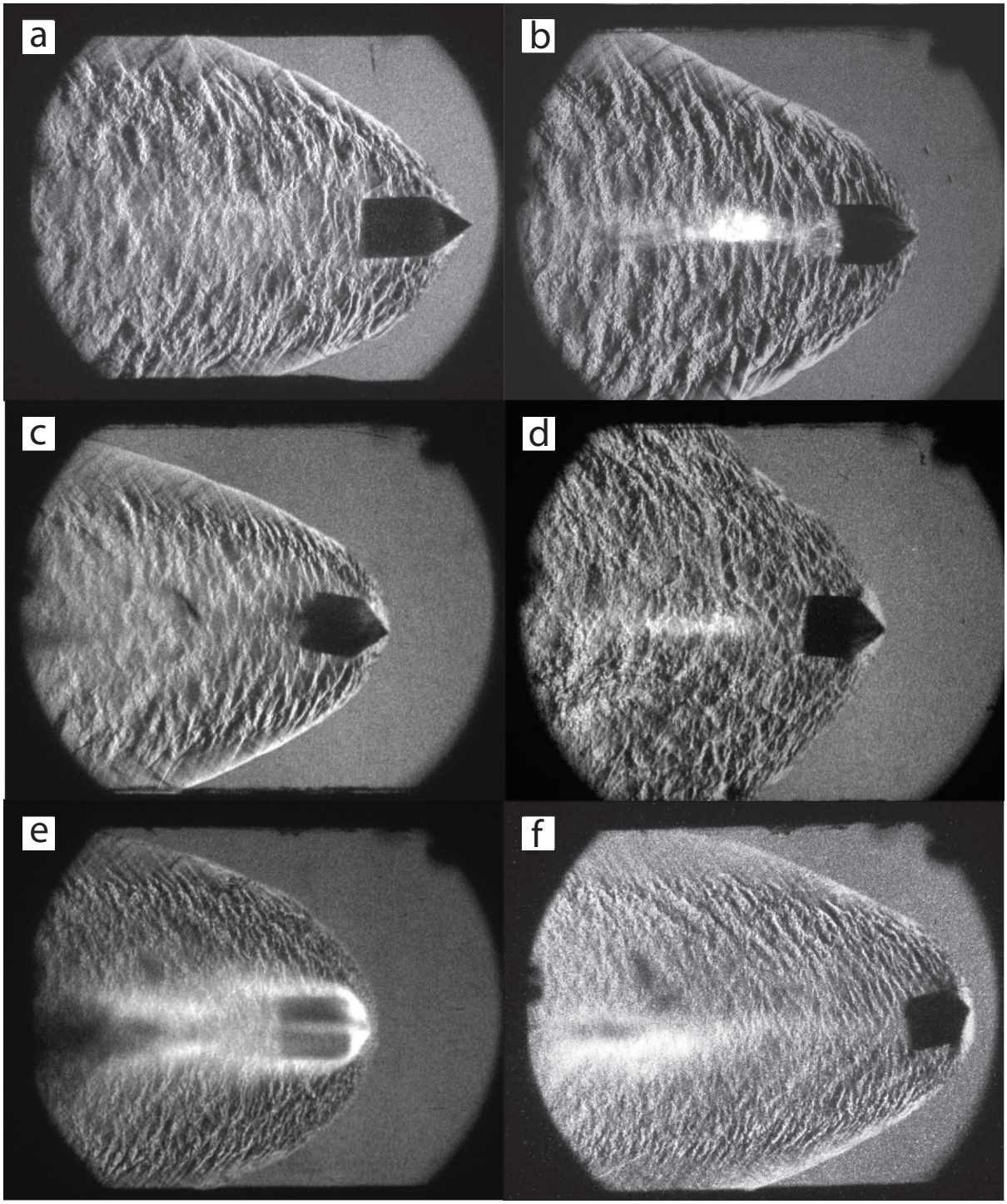

Figure 2: Schlieren photographs: a) 35° projectile moving at 1 790 m/s into 81 kPa mixture, b) 45° projectile moving at 1 720 m/s into 97 kPa mixture, c) 45° projectile moving at 1 850 m/s into 61 kPa mixture, d) 45° projectile moving at 2 150 m/s into 80 kPa mixture, e) 60° projectile moving at 1 870 m/s into 76 kPa mixture, f) 60° projectile moving at 1 980 m/s into 65 kPa mixture.

produced by the smallest cone half angle (35°) is displayed in Fig. 2a. Large density gradients can be observed and decoupling of the pulsations from the oblique shock occurs above and below the projectile. Similar instabilities from a 45° cone half angle are shown by Figs. 2b,c. In Fig. 2d, the pulsations remain coupled to the oblique shock in the entire field of view. This case is at the boundary of initiating an oblique detonation wave. In Figs. 2e,f, combustion instabilities induced from 60° cone half angle projectiles are illustrated. For these cases, the pulsation frequency is higher than that of the smaller cone angles.

All the flowfields shown in Fig. 2 correspond qualitatively to the large-disturbance regime, since they exhibit irregular low-frequency pulsations. From these experiments, the first Damköhler number can be calculated and compared with previous results related to spherical-nosed projectiles. For the cases where the oblique shock is attached at the tip of the cone (Figs. 2a,b,c,d), an inert conical shock is considered, behind which the flow is modeled by a Taylor-Maccoll algorithm. The parameters a_2 and T_2 are thus the average between the values behind the conical shock and the cone surface. For the cases where the shock is detached in front of the cone (Figs. 2e,f), a bow shock is considered; a_2 and T_2 are calculated behind a normal shock, similar to the case of a blunt-nosed projectile. The fluid time scale, chemical time scale and first Damköhler number for the 6 experiments are provided in Table 1.

Table 1: Experimental conditions and Damköhler number for the cases shown in Fig. 2

Case	Experimental conditions			τ_f	τ_c	Da
	Velocity (m/s)	Pressure (kPa)	cone half angle (°)	(μs)	(μs)	
a	1 790	81	35	18.1	0.469	38.6
b	1 720	97	45	15.8	0.450	35.1
c	1 850	61	45	15.0	0.461	32.5
d	2 150	80	45	13.3	0.561	23.7
e	1 870	76	60	12.4	0.161	77.0
f	1 980	65	60	11.8	0.212	55.7

In Table 2, the Damköhler numbers from previous investigations related to spherical-nosed projectiles are presented. From these experiments, Matsuo and Fujii [11] concluded that the regular regime occurred for $Da < 80$ and the large-disturbance regime was identified for $Da > 80$, which was also in accordance with their numerical simulations. According to the results of the present investigation, the classification of the combustion instabilities produced by conical projectiles using the first Damköhler number does not agree with the classification of the combustion instabilities produced by spherical-nosed bodies. The large-disturbance regime around conical projectiles occurred for $20 < Da < 80$. In the case of spherical-nosed projectiles, the regular regime occurred for $Da < 80$ and the large-disturbance regime was observed for $Da > 80$.

Table 2: Damköhler number for previous studies related to spherical-nosed projectiles

Case	Experiment	Velocity (m/s)	Pressure (kPa)	Da	Regime
g	Lehr [2]	1685.0	42.66	77.64	regular
h	Lehr [2]	1931.0	42.66	77.42	regular
i	Ruegg and Dorsey [1]	1758.6	50.66	128.06	large disturbance
j	Ruegg and Dorsey [1]	1963.2	50.66	127.82	large disturbance

Possible explanations for this discrepancy consist of a curvature effect of the detonation front around the flight axis and the fact that the one-dimensional wave interaction model is no longer valid for conical flows. Figure 3 shows a schematic of the combustion instabilities around spherical and conical bodies, where the shock and the reaction fronts are displayed. For the spherical case, the wave interaction model is applied along the stagnation streamline. In the conical case, the model can no longer be applied at the axis of symmetry and a two-dimensional (axisymmetric) model is required. Furthermore, the combustion pulsations occur in a region where the curvature of the shock front can be significant. Such curvature can potentially enhance the ignition and failure mechanisms and thus alter the combustion instabilities.

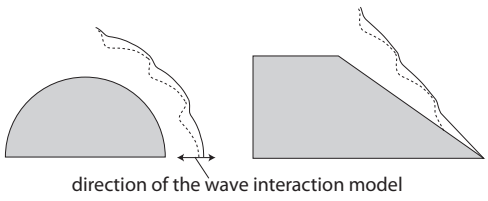

Figure 3: Schematic of the combustion instabilities around spherical and conical bodies.

5 Conclusion

Conical projectiles were launched into a combustible gaseous mixture and Schlieren photographs revealed the generation of combustion instabilities in the form of the large-disturbance regime. By comparing the results with previous investigations where spherical-nosed projectiles were used, the first Damköhler number can not be used to predict the type of combustion instabilities. Instead, a two-dimensional model needs to be developed and the role of the shock front curvature has to be assessed.

References

[1] Ruegg FW, Dorsey WW (1962) J. of Research of the Nat. Bur. of St. C. Eng. and Instr. 66C: 51.

[2] Lehr HF (1972) Astro. Acta. 17: 589.

[3] Alpert RL, Toong TY (1972) Astro. Acta. 17: 539.

[4] McVey JB, Toong TY (1971) Combust. Sc. and Tech. 3: 63.

[5] Matsuo A, Fujiwara T (1991) Prog. in Astro. and Aero. 154: 516.

[6] Matsuo A, Fujii K (1995) AIAA J. 33: 1828.

[7] Ahuja JK et al (1996) J. of Prop. and Power. 12: 518.

[8] Sussman MA (1994) A computational study of unsteady shock induced combustion of hydrogen-air mixtures. 30th AIAA/ASME/SAE/ASEE Joint Prop. Conf.

[9] Matsuo A et al (1995) AIAA J. 33: 1056.

[10] Yungster S, Radhakrishnan K (1996) Shock Waves. 5: 293.

[11] Matsuo A, Fujii K (1998) AIAA J. 36: 1834.

[12] Toong TY (1983) Combustion dynamics: the dynamics of chemically reacting fluids. McGraw-Hill.

[13] Kasahara J (1996) Symp. (Int.) on Combust. 26: 2903.

[14] Development of a detonation-driven gas gun capable of 3 km/s projectile velocity. 27th Int. Symp. on Shock Waves.